Organic Electronics 10 (2009) 551–561

Contents lists available at ScienceDirect

Organic Electronics

journal homepage: www.elsevier.com/locate/orgel

All-solution-processed inverted polymer solar cells on granular surface-nickelized polyimide

Yu-Sheng Hsiao [a], Chih-Ping Chen [b], Ching-Hsun Chao [c], Wha-Tzong Whang [a,*]

[a] Department of Materials Science and Engineering, National Chiao Tung University, Hsinchu 300, Taiwan, ROC
[b] Material and Chemical Research Laboratories, Industrial Technology Research Institute, Hsinchu 300, Taiwan, ROC
[c] Department of Materials Science and Engineering, Mingdao University, Chang-Hwa, Taiwan, ROC

ARTICLE INFO

Article history:
Received 14 December 2008
Received in revised form 22 January 2009
Accepted 23 January 2009
Available online 3 February 2009

Keywords:
All-solution-process
Inverted polymer solar cells
PEDOT/PSS

ABSTRACT

In this study, we prepared all-solution-processed inverted polymer solar cells (PSCs) incorporating two solution-processed electrodes – surface-nickelized polyimide films (NiPI films) as cathodes and high-conductivity poly(3,4-ethylenedioxythiophene)/poly(styrenesulfonate) (PEDOT:PSS) films as anodes – and an active layer with a bulk heterojunction morphology of poly(3-hexylthiophene) (P3HT) and [6,6]-phenyl-C_{61}-buytyric acid methyl ester (PCBM). The granular Ni thin films, which exhibited good adhesion and high-conductivity (ca. 2778 S cm^{-1}) on the polyimide (PI) substrates and possessed a work function different from that of pure Ni metal (WF, 5.4 eV). Using ultraviolet photoelectron spectroscopy, we determined that the WF of the NiPI films was ca. 3.9 eV. Prior to the coating of the photoactive layer, the surface of the NiPI films were treated with titanium(diisopropoxide)bis(2,4-pentanedionate) (TIPD) solution to facilitate the deposition of high-quality active layer and further as a hole blocking layer. The solution processed anodes (solvent-modified PEDOT:PSS films) were further coated and subjected to mild oxygen plasma treatment on the active layer. Short exposure (5 s) to the plasma improved the quality of the surface of the active layer for PEDOT:PSS deposition. These inverted PSCs on flexible granular NiPI films provided a power conversion efficiency of 2.4% when illuminated under AM 1.5 conditions (100 mW cm^{-2}). The phenomenon of light absorption enhancement in those inverted PSCs was observed as indicated in reflective UV–vis, haze factor and external quantum efficiency (EQE) responses. The resulting fill factor (FF) of 0.43 is still significantly lower than the FF of 0.64 for standard devices. When compared to the planar structure, the improvement of absorbance of light and good haze factors was obtained for granular structure which suggests NiPI as a better back contact electrode through enhancing the light trapping and scattering in inverted PSCs.

1. Introduction

Polymer solar cells (PSCs) have recently received considerable attention because of their low cost, light weight, high flexibility, and solution-processability. The power conversion efficiency (PCE) of PSCs has been improved to 5% under AM 1.5G conditions [1–4] when using a bulk heterojunction (BHJ) structure comprising a blended film of poly(3-hexylthiophene) (P3HT) as the donor and [6,6]-phenyl-C_{61}-butyric acid methyl ester (PCBM) as the acceptor. In addition to their improved device efficiency [1–5] and lifetime [6,7], PSCs possessing inverted structures have also been investigated to further reduce production costs and to facilitate high-throughput production [8–22]. Among inverted PSCs, two major structures are studied most frequently. One employs modified layers located between the active layer and the electrodes to change the energy level of the whole device, i.e., the roles of the indium tin oxide (ITO) material (as the cathode) and the metal

* Corresponding author. Tel.: +886 35 731873; fax: +886 35 724727.
E-mail address: wtwhang@mail.nctu.edu.tw (W.-T. Whang).

1566-1199/$ - see front matter © 2009 Elsevier B.V. All rights reserved.
doi:10.1016/j.orgel.2009.01.012

electrode (as anode) are different from those of standard PSCs systems [ITO (anode)/PEDOT:PSS/active layer/metal (cathode)] (Fig. 1A). For this inverted system, in which the roles of the electrodes are exchanged, the use of solution processing methods results in enhanced efficiency from the collocation of appropriate energy levels for the electron- and hole-collection layers [8–14]; in addition, a roll-to-roll suited module would be achieved when introducing an inject-printed metal as the anode (Fig. 1B). The second type of inverted PSC possessing a layer sequence has great promise for use as a cost-efficient roll-to-roll suited module, i.e., starting with the metallic electron contact on a plastic substrate [16–23]. The active layer is coated on the metal layer, followed by the PEDOT:PSS layer, which forms the transparent hole contact. In this inverted system, the roles of the anode and cathode are similar to those in standard cells, but the processing method employed to build the PSCs is different (Fig. 1C). Moreover, the preparation of this second type of inverted PSC would presumably provide higher efficiency and lower device fabrication costs when using ITO-free materials. Another advantage when using this inverted PSC system [22,23] with high topographical variations of metals is that it would lead to an imposed topography on the photovoltaic device; it could also be used to couple light into the film, increasing the optical length in the device. Based on these previous studies, we suspected that combining the technologies for all-solution processing with the high topographical variations of the metal and the high-conductivity of PEDOT:PSS would allow us to obtain ITO-free inverted PSCs for high-throughput production on flexible substrates.

Recently, polyimide (PI) films have become generally used components for flexible electronic devices because they exhibit high glass transition temperatures, low surface roughnesses, low coefficients of thermal expansion (CTE), and high chemical resistance under typical fabrication conditions. Surface-metalized PIs have been developed widely using various metals, including Ag, Cu, and Ni [24–27]. In a previous study [26], we developed an all-solution method for fabricating thin granular Ni films on PI (NiPI) with high adhesion and conductivity (ca. 2778 S cm^{-1}). These NiPI films are readily fabricated through alkaline hydrolysis to open the imide rings of the pristine PI film, followed by ion exchange with Ni ions and their subsequent reduction on the PI (Fig. 2A–E).

In this paper, we report the fabrication of all-solution-processed inverted PSCs featuring NiPI as the cathode material (back contact electrode) on flexible substrates; these devices have the following configuration: PI/Ni (cathode)/titanium(diisopropoxide)bis(2,4-pentanedionate (TIPD)/P3HT:PCBM/PEDOT:PSS (anode). From the many reports describing the insertion of a buffer layer between the cathode and the active layer to improve device performances [4,28–30], we chose the solution-processable TIPD as the buffer layer in this study because Tan et al. [30] demonstrated that the TIPD interface dramatically reduces the degree of interface resistance between the cathode and the active layer. Furthermore, because the energy level of the lowest unoccupied molecular orbital (LUMO) of TIPD is ca. 3.9 eV, we suspected that it would be easy to transport electrons to the NiPI film [work function (WF) = 3.9 eV]. In addition, we developed a low-temperature fabrication process (<150 °C) to obtain high-conductivity PEDOT:PSS films in these inverted ITO-free PSCs. We readily obtained these high-conductivity PEDOT:PSS films (ca. 283 S cm^{-1}) through spin-coating of a solvent (methoxyethanol, ME) onto pre-coated PEDOT:PSS films [31]; this method appears to be more suitable for plastic substrates because it does not require a very high-temperature (>150 °C) to remove any polyalcohol [32–37] and, thereby, decreases the likelihood of destroying the active layer. Based on the previous report, [31] the sheet resistance of PEDOT:PSS electrode (a distance effect for PED-

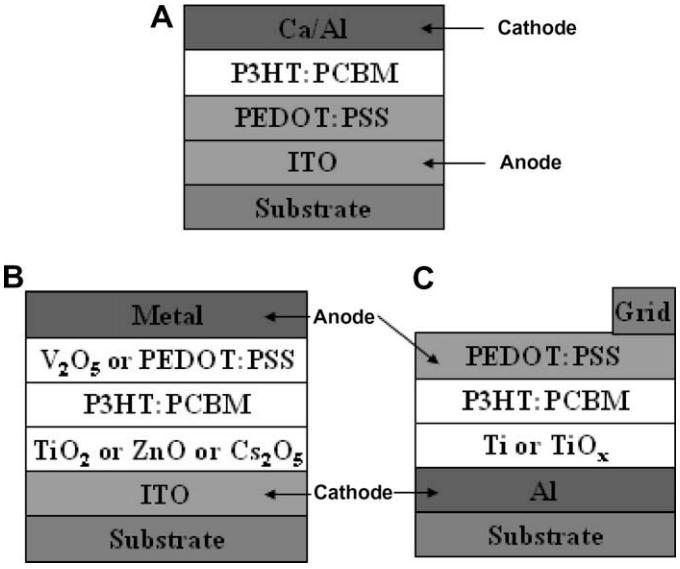

Fig. 1. Architectures of polymer solar cells: (A) standard, (B) inverted (in terms of the roles of the electrodes), and (C) inverted (in terms of the alternative processing structure).

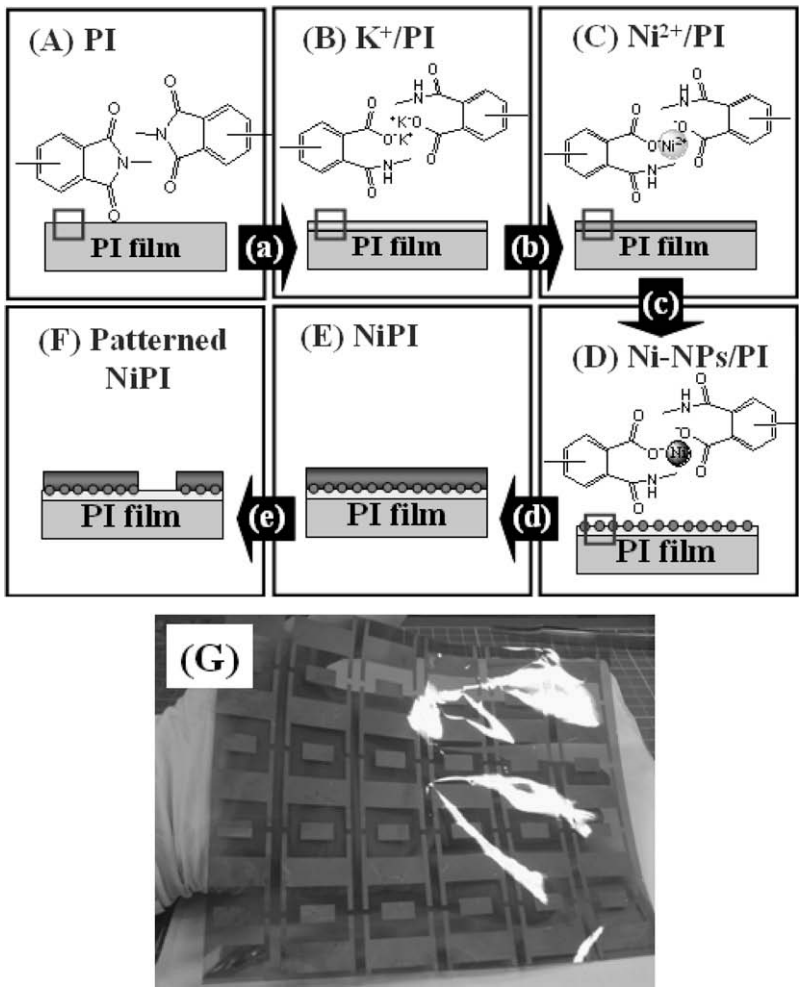

Fig. 2. Flow chart for the formation of the patterned NiPI film. (A) PI: pristine polyimide; (B) K^+/PI: K^+/PAA layer on PI film; (C) Ni^{2+}/PI: Ni^{2+}/PAA layer on PI film; (D) Ni-NPs/PI: Ni-NPs/PAA layer on PI film; (E) NiPI: Ni/PAA layer on PI film; (F) Patterned NiPI: patterned Ni/PAA layer on PI film; (G) photograph of the patterned NiPI. (a) Alkaline hydrolysis to open imide rings; (b) cation-exchange reaction leading to the incorporation of Ni^{2+} ions; (c) reduction of Ni^{2+} ions by aqueous $NaBH_4$; (d) Ni electroless plating using an EN solution; (e) patterning of Ni through photolithography.

OT:PSS based ITO-free PSC devices) increased as the area of the device increasing, and hence decreased the device performance. The low conductivity of the PEDOT:PSS electrode is actually limited for larger area cells. Therefore, we further deposited a Au grid (thickness at 100 nm) onto the PEDOT:PSS films to efficiently collect holes and efficiently increase the sheet conductivity of the transparent electrode.

2. Experimental

2.1. Nickelized polyimide films (cathodes and substrates)

The process for the direct all-wet-chemical treatment of Ni-coated conductive films was performed according to the procedure outlined in Fig. 2A–F. The PI films were synthesized from pyromellitic dianhydride (PMDA; from TCI) and 4,4′-diaminodiphenylether (ODA, 98%; from Aldrich); the experimental details for fabricating the PI and nickelized PI films are available elsewhere [26]. Briefly, the PI films were first immersed in 5 M aqueous KOH at 25 °C for 7 min and then rinsed with deionized water. Next, the K^+ counterions associated with the opened imide rings on the surface of the PI films were exchanged with Ni^{2+} ions through immersion in 50 mM aqueous nickel sulfate at 25 °C for 5 min, followed by rinsing with deionized water. The surface Ni^{2+} ions were then reduced in aqueous $NaBH_4$ (0.2 g/100 ml deionized water) at 25 °C for 5 min to form Ni nanoparticles on the PI surface (Ni-NPs/PI films), which were then rinsed with deionized water. The Ni NP-seeded PI films were immersed in an electroless nickel bath (EN solution) at 50 °C for 8 min to form thin Ni layers on the PI films (NiPI). The EN solution was prepared from a 4:1 (v/v) mixture of a Ni stock solution [nickel sulfate ($40\ g\ l^{-1}$), sodium citrate ($20\ g\ l^{-1}$), and lactic acid ($10\ g\ l^{-1}$) in deionized water) and a DMAB solution ($1\ g\ l^{-1}$ in deionized water). A cartoon representation and a photograph of the patterned NiPI are presented in Fig. 2F and G, respectively. The NiPI films have long-term air stability in the atmosphere. Prior to the deposition of

the photoactive layer, the NiPI films were cleaned with organic solvents.

2.2. Active-layer materials

Because of the large differences in the values of the contact angles and surface energies of Ni and PI surfaces (Table 1), the solution-processable titanium chelate TIPD (from Aldrich) was pre-coated as the cathode buffer layer on the patterned NiPI film surfaces to facilitate the fabrication of high-quality active layers. Next, a blend [1:0.8 (w/w), 17 mg ml^{-1} in dichlorobenzene (DCB)] of P3HT (Rieke Met. Inc.) and PCBM was stirred overnight in DCB, filtered through a 0.2 μm poly(tetrafluoroethlene) (PTFE) filter, and then spin-coated (500 rpm, 60 s) on top of the NiPI films.

2.3. High-conductivity PEDOT:PSS films (anodes)

The high-conductivity PEDOT:PSS anodes were prepared using a two-step method [31]. In the first step, a 95:5 (w/w) mixture of PEDOT:PSS solution (HC V4; from H. C. Starck) and dimethyl sulfoxide (DMSO; from Aldrich) was filtered through a 0.45 μm filter prior and then deposited (spin-coating at 4000 rpm in the air) onto the active layers with a mild oxygen plasma exposure for 5 s (plasma cleaner PDC-32G, Harrick Scientific, Ossining, NY) at a thickness ca. 50 nm. In the second step, the surface-modifying solvent, ME, was spin-coated onto the pristine PEDOT:PSS films at 3000 rpm, which were then dried at 100 °C for 5 min inside a glove box. The device was completed by coating a 100 nm-thick layer of Au as a metal grid and a mask to improve hole-collection and define the active area, respectively. The cell was then encapsulated using UV-curing glue (Nagase, Japan). The active area of each photovoltaic (PV) cell was 0.036 cm^2. Fig. 4A displays the architecture of the inverted ITO-free polymer/fullerene solar cells.

2.4. Instrumentation

The NiPI films were transferred within 3 min of their formation into the sample-loading chamber of an ultraviolet photoelectron spectroscopy (UPS) system. UPS (VG ESCALab 250, HeI $h\nu$ = 21.2 eV) spectra were recorded at a sample bias of −5.0 V to observe the secondary electron cutoff, from which the work function could be derived from the width of the Fermi edge of a Au substrate. XPS spectra were recorded using a VG Scientific Microlab 350 spectrometer operated in the constant analyzer energy mode with a pass energy of 50 eV and Mg · Kα (1253.6 eV) radiation as the excitation source (with normal emission detected). The sheet resistances of the PEDOT:PSS films were measured using a four-point probe; the average of the measured values is reported. The transmittance spectra were recorded using an HP8453 UV–vis spectrometer. Contact angles and surface energies were measured and calculated using the geometric mean approximation (GMA) and a FTA-200 dynamic contact analyzer operated with H_2O and CH_2I_2 as the two standard liquids. The crystalline phase of samples was characterized using a BEDE D1 grazing incidence X-ray diffractometer (GIXRD) and Cu · Kα radiation. The incident angle of the X-ray beam was fixed at 0.5°. The surface morphologies and phase changes of the PEDOT:PSS films were analyzed using a VEECO DICP-II atomic force microscope (AFM) operated in the tapping mode (Si tips on Si cantilevers having a spring constant of 2 N m^{-1} and a set point of ca. 0.8–0.9) in the air. A JEOL JSM-6500F scanning electron microscope (SEM) was employed to investigate the thicknesses of the PEDOT:PSS films. Samples for transmission electron microscopy (TEM) analysis were prepared through microtoming with a Leica Ultracut Uct apparatus into 90 nm-thick slices that were placed onto a 200-mesh carbon-coated Cu TEM grid (Agar Sci., Inc.). TEM images were recorded using a JEOL-2010 transmission electron microscope and an internal charge-coupled device (CCD) camera. Current–voltage (I–V) curves of the PSC devices were measured using a computer-controlled Keithley 2400 source measurement unit (SMU) equipped with a Peccell solar simulator under AM 1.5 illumination (100 mW cm^{-2}). The spectral irradiance data of the light source was similar to the AM 1.5G solar spectrum (spectral mismatch <5% in the range 350–800 nm). The illumination intensity was calibrated using a standard Si photodiode detector equipped with a KG-5 filter. All of these measurements were performed under an ambient atmosphere at room temperature. All of these inverted PSCs are identified by "PTXNiPI-X", the first number denoting to the incorporating different concentrations of TIPD (wt%), the follow number denoting to the thermal annealing time (min). The absorption spectra were recorded using a Hitachi U-4100 UV–vis spectrometer with the integrating sphere. The planar and granular substrates were characterized by optical spectrometry (MFS-530 commercialized by Hong-Ming Technology): the total and scattered reflectivity have been measured and the haze factors ($H_R(\lambda)$) have been calculated for each of the substrates according to the equation, $H_R(\lambda)$ = Rscat(λ)/Rtot(λ), and these optical measurements have been performed in air.

Table 1
Contact angles and surface energies obtained after performing the inverted fabrication process.

Sample	H_2O	$C_2H_4I_2$	Surface energy (mJ m^{-2})
PI	75.5	41.1	39.1
NiPI	104.9	38.0	58.4
TNiPI	87.0	33.6	46.6
PTNiPI	108.2	60.6	37.0
PTNiPI[a]	55.8	32.7	47.4
HCV4	48.0	29.5	52.1

PI: Pristine polyimide film.
NiPI: Ni/PI film obtained after annealing at 150 °C for 30 min.
TNiPI: Sample obtained after depositing TIPD solution on the NiPI and then annealing at 70 °C for 5 min.
PTNiPI: Sample obtained after depositing the P3HT:PCBM film on the TNiPI and then annealing at 140 °C for 15 min.
HCV4: Sample obtained after depositing the PEDOT:PSS film on the glass substrate and then annealing at 100 °C for 5 min.
[a] After mild air plasma treatment for 5 s.

3. Results and discussion

To examine the feasibility of using NiPI as the cathode (back contact electrode), we used UPS to determine that

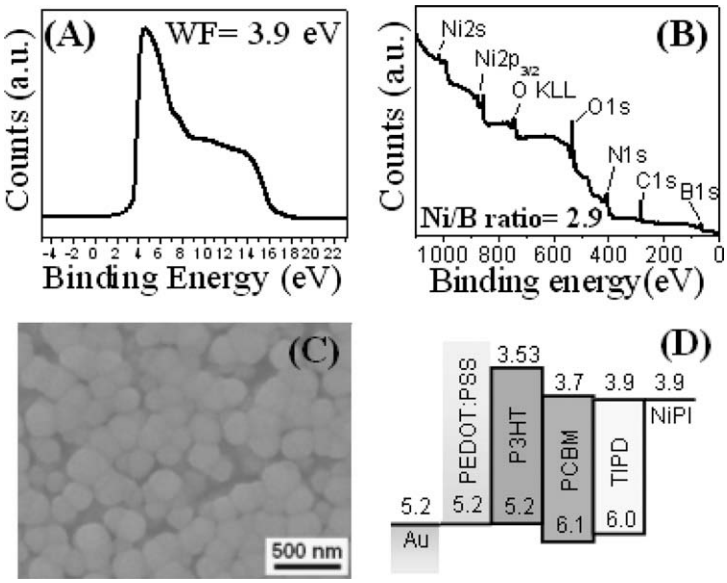

Fig. 3. (A) Photoelectron spectrum of NiPI film. (B) XPS spectrum of NiPI surface. (C) SEM image of NiPI surface. (D) Schematic representation of the energy levels of an ITO-free inverted PSC on PI.

the WF of the surface-nickelized PI (NiPI) was 3.9 eV, i.e., it differs from that of pure Ni (Fig. 3A) [38]. Because this value is lower than that of the Al cathode (ca. 4.2 eV), it appeared suitable for application as the back contact electrode in inverted PSCs. To understand why there was a difference in the WFs of NiPI and pure Ni, we performed an XPS survey and then obtained the Ni/B ratio of NiPI (ca. 2.9) by using the Shirley method to estimate the peak areas of the atom contents on the NiPI surface in Fig. 3B. According to previous reports [26,27] and the results of this XPS analysis, in addition to a small amount of oxygen (representing native oxides or B_2O_3) formed on the NiPI surface, we suspect that the Ni–B component, which arose from the use of dimethylamine borane (DMAB) as the reductant in the Ni electroless deposition process, was responsible for the WF of the NiPI film to differ from that of pure Ni. The SEM image in Fig. 3C reveals that the granular NiPI consisted of fine particles (ca. 200–300 nm) with a continuous and interconnected network. Fig. 3D provides a schematic energy level diagram. The WF of NiPI allows efficient electron transfer from the LUMO of PCBM. Based on the previously report [30], the TIPD layer could improve the electron collection and reduce the interface resistance between the active layer and the metal cathode. From the view of energy level, the WF of TIPD matches the transport levels of the respective charge carriers for efficient charge transferring, however, other effects like oxide layers, dipole layers or the interface morphology of the photoactive layer might affect the charge injection. Table 1 summarizes the contact angle (CA) and surface energy (SE) data. On the surface of patterned NiPI, the difference in the H_2O contact angles of PI (CA = 75.5°) and Ni (CA = 104.9°) was dramatic. We attempted to improve the device performance through solvent annealing (slow drying) with DCB, a solvent with a high-boiling-point, to enhance the degree of microcrystalline lamellar stacking in the solid state packing of the active layer [39]. We found, however, that the slow drying process had a negative effect on the quality of the P3HT:PCBM film when using the patterned NiPI as the substrate. After spin-coating the P3HT:PCBM solution onto the patterned NiPI film, droplets of P3HT:PCBM tended to aggregate on the Ni surface through slow growth and the thickness of the active layer became non-uniform. To overcome this problem, we pre-coated the TIPD onto the NiPI surface. The TIPD-modified, patterned NiPI film, which we refer to as TNiPI, had a contact angle of 87.0°; therefore, droplets of the P3HT:PCBM solution covered the TNiPI surface more completely, resulting in uniform P3HT:PCBM films that we name PTNiPI.

Because of the large variation in the values of CA of P3HT:PCBM and PEDOT:PSS (Table 1), the deposition of PEDOT:PSS on the highly hydrophobic P3HT:PCBM surface requires a preliminary treatment process to ensure wettability and adhesion. Chaudhary et al. [40] demonstrated that short exposure (5 s) to Ar plasma can effectively tailor the wettability of P3HT:PCBM layers for subsequent deposition of single-wall carbon nanotubes (SWNT) from an aqueous solution. In our present study, oxygen plasma treatment was more convenient than Ar plasma treatment; therefore, we subjected our PTNiPI film to a short (5 s exposure) oxygen plasma treatment to facilitate the deposition of PEDOT:PSS on the active layer. The oxygen plasma-treated PTNiPI film exhibited values of CA and SE of ca. 55.8° and 47.4 mJ m^{-2}, respectively, similar to those of the PEDOT:PSS film. To determine the influence of the 5 s oxygen plasma treatment on the surface of the active layer, we analyzed the performance of standard PSC structures (glass/ITO/PEDOT:PSS/P3HT:PCBM/Ca/Al) formed with and without plasma treatment. The variation in the PCE was less than ca. 0.1%, arising mostly from a slight loss in the current density; the values of V_{oc} and the fill factor (FF) were unaffected, as revealed by the *I–V* characteristics

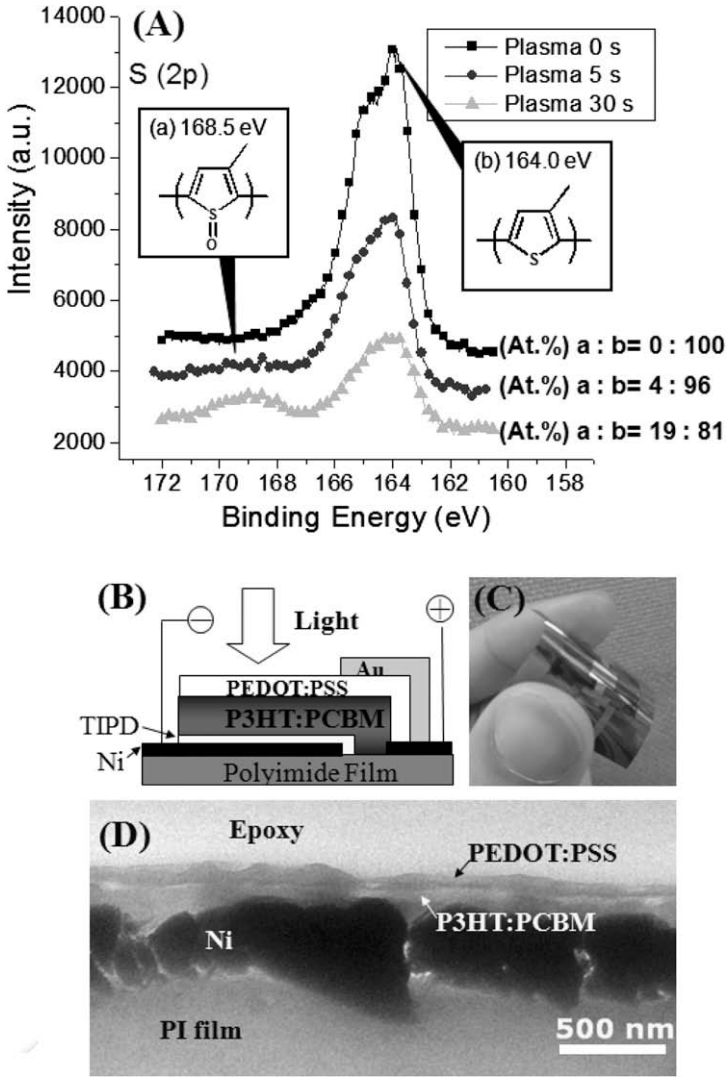

Fig. 4. (A) S(2p) core level spectra of P3HT:PCBM film (1:0.8 w/w) with plasma treatment for various seconds. (B) Architecture of an inverted PSC featuring an inverted sequence on NiPI as the back contact electrode. (C) Optical image of an inverted PSC on NiPI. (D) TEM cross-sectional image of an inverted PSC on NiPI. Scale bars, 500 nm.

Table 2
Sheet resistances and conductivities of PEDOT:PSS, ITO, and NiPI films.

Sample	Film thickness (nm)	Transmittance at 550 nm (%)	Sheet resistance[c] (kΩ sq^{-1})	Conductivity[c] (S cm^{-1})
H	90[a]	96.7	22.00	5
HD	45[a]	96.9	1.310	170
HDM	45[a]	96.4	0.785	283
ITO	200[a]	89.6	0.007	7143
NiPI	300[b]	–	0.012	2778

H: Thin film of PEDOT:PSS (HCV4) on the glass substrate.
HD: Thin film obtained from a mixture of HCV4 (95 wt%) and DMSO (5 wt%) on the glass substrate.
HDM: ME-modified HD thin film on the glass substrate.
[a] Film thickness identified using SEM.
[b] Film thickness identified using TEM.
[c] Values determined using a four-probe point.

(Table 3). The treatment of oxygen plasma might predominately destroy the P3HT phase, but not the PCBM phase. As the consequence, the electron injection interface might still be working for standard cell. However, this may significant effect the anode interface. To investigate if and how the effect through oxygen plasma treatment, we employed XPS measurements to quantitative determine the thiophene defects through oxygen plasma treatment (Fig. 4A). The S(2p) core level spectra showed that there were 96% thiophene (at 164 eV) preserved and only 4% thiophene defects (at 168.5 eV) were observed through 5 s oxygen plasma treatment on the active layer surface. In the inverted geometry, this would lead to a destruction of the anode interface; however the effect is not significant as a result of XPS spectra.

To apply PSCs in an economical roll-to-roll-suited module, the major requirement to reduce the cost of produc-

Table 3
Performance of PSCs under AM 1.5 illumination (100 mW cm^{-2}).

Sample	Structure	J_{sc} (mA cm^{-2})	V_{oc} (V)	FF	PCE (%)
Standard[a]	Standard	9.2	0.64	0.63	3.7
Standard-p[a]	Standard	8.8	0.63	0.64	3.6
PT1NiPI-5[b]	Inverted	8.3	0.58	0.26	1.2
PT3NiPI-5[b]	Inverted	9.0	0.54	0.29	1.4
PT0NiPI-15[b]	Inverted	5.4	0.43	0.25	0.6
PT1NiPI-15[b]	Inverted	9.2	0.59	0.37	2.0
PT3NiPI-15[b]	Inverted	9.3	0.60	0.43	2.4
PT7NiPI-15[b]	Inverted	5.2	0.61	0.35	1.1
PT15NiPI-15[b]	Inverted	4.4	0.59	0.24	0.6

Standard: Standard PSC structure without plasma treatment.
Standard-p: Standard PSC structure with plasma treatment on the active layer.
[a] Active area = 0.04 cm^2.
[b] Active area = 0.036 cm^2.

tion is substitution of a cheap material in place of the ITO electrode. In a previous report, Zimmermann et al. [18] constructed an ITO-free PSC module that comprised PSCs on metal-coated plastic substrates with an inverted layer sequence. Based on their module concept, we examined the solution processing of NiPI, our surface-nickelized PI film, as the cathode/substrate and the high-conductivity PEDOT:PSS as the anode for the all-solution processing of PSCs (Fig. 4B). Fig. 4B–D presents the structure, optical and TEM images of the inverted PSC cell on NiPI. Although the TIPD layer was too thin to identify, the cross-sectional TEM image of the device clearly indicates the presence of individual layers without interlayer mixing (Fig. 4D). The PSCs had the following device structure: PI/Ni (385 nm ± 77 nm)/TIPD/P3HT:PCBM (100 nm)/PEDOT:PSS (45 nm).

The conductivity of NiPI and ITO were 2778 and 7143 S cm^{-1}, respectively (Table 2). The resistive loss of NiPI could be ignored for small cell device. Nonetheless, NiPI layer is actually limited for larger area cells similar to the ITO based devices. To form a transparent conducting anode, we employed the low-temperature processing of high-conductivity PEDOT:PSS. When processing with a polyalcohol, the conductivity of PEDOT:PSS films can be enhanced for their application in PSCs. Although adding a polyalcohol would obviously decrease the sheet resistance of the PEDOT:PSS films, higher processing temperatures (>140 °C) and longer thermal treatment times are necessary to remove the high-boiling-point (>200 °C) additive [32–37], which may damage the P3HT/PCBM blends in our inverted structure. Herein, we selected DMSO and ME as solvents to investigate their ability to enhance the conductivity of PEDOT:PSS at low processing temperatures. The pristine PEDOT:PSS film (H; HC V4 from H. C. Starck) had the lowest conductivity (5 S cm^{-1}). When we added 5 wt% DMSO into this pristine PEDOT:PSS aqueous solution, the conductivity of the HD film was enhanced to 170 S cm^{-1}. Furthermore, consistent with our results from a previous study [31], surface solvent-treatment of HD films with ME (HDM) led to a dramatic increase in the conductivity of the PEDOT:PSS to 283 S cm^{-1} and a corresponding processing temperature lower than that required for the polyalcohol system.

If transparent electrodes are to be used in PV devices, they must have high transparency in the visible region. Thicker PEDOT:PSS films will lead to transmittance and vertical conductivity problems. We observed that the transmittances of the thin PEDOT:PSS films (<100 nm) of H, HD, and HDM on glass (each ca. 96%) were better than that of ITO (ca. 89.6%; Table 2). From a comparison of the electrical conductivities of ITO (same as the anode of a standard cell), and NiPI, we observed that the highest conductivity of PEDOT:PSS (HDM) was enhanced to 283 S cm^{-1} with a order less than ITO and NiPI. We suspect that combining a suitable metal grid (such as a metal grating or random metal nanowire mesh) with HDM film may be compatible with the future development of flexible PSCs [41,42].

Because TIPD was present as an ultrathin layer on NiPI (Fig. 4D), it was necessary for us to determine the thickness of P3HT:PCBM on the highly topographically variant NiPI to obtain the optimized parameters for these inverted PSCs, because the effect of a thinner active layer (higher speed of coating of the P3HT:PCBM solution) on the imposed topography of the anode would increase the risk of creating short circuits (i.e., lower the efficiency of the device) [22]. If the P3HT:PCBM solution was spin-coated on TNiPI for 700 rpm, the thinner active layer film on the imposed topography of anode would increase the risk of creating short circuits to lower the efficiency of the device. As the result of the device performance and the TEM cross-sectional image, the minimum active layer film thickness was suggested to be ca. 200 nm. Thus, under the optimal conditions for spin-coating of the P3HT:PCBM solution onto TNiPI (500 rpm), we investigated the concentrations with respect to the thickness of the TIPD layer of the whole devices. Prior to the coating of the photoactive layer, the TIPD layers were treated at the temperature of 80 °C and 160 °C for 5–30 min to investigate the temperature effect of the TIPD film without a superimposed effect of the active layer. Similar cell performances were obtained as the temperature and annealing condition change. First, to understand the thermal stability of the TIPD-coated devices, we examined the device performances after employing various thermal annealing times. Table 3 summarizes the device performance under AM 1.5 illumination at an intensity of 100 mW cm^{-2}. The device formed using an interfacial layer of 3.75 wt% TIPD (PT3NiPI-5) and a short thermal annealing time (5 min; 140 °C), exhibited poor performance: V_{oc} = 0.54 V; J_{sc} = 9.0 mA cm^{-2}, FF = 0.29; PCE = 1.4%. After increasing the thermal annealing time at 140 °C to 15 min, the values of V_{oc}, J_{sc}, and FF all increased, thereby improving the value of PCE to 2.4%. When TIPD was incorporated at 1.88 wt% (PT1NiPI-15), we obtained similar results, i.e., improved performance after longer periods of thermal treatment; after thermal annealing for 15 min, the values of V_{oc}, J_{sc}, FF, and PCE were 0.59 V, 9.2 mA cm^{-2}, 0.37, and 2.0%, respectively. Consistent with previous results, this TIPD-coated NiPI was stable to thermal annealing at 140 °C for several minutes. We suspect that this TIPD-coated NiPI would be more suitable than the corresponding ITO/PET system [43,44] for long-time high-temperature annealing.

To compare the performance of devices incorporating different concentrations of TIPD (0.94, 1.88, 3.75, 7.5, and 15 wt%), we performed AFM measurements to determine the underlying mechanism of TIPD incorporation on NiPI. We observed interesting morphologies with high topographical variations for the pristine NiPI and TIPD-coated NiPI surfaces (Fig. 5). After coating with TIPD at 0.94, 3.75, and 15 wt%, the root-mean-square roughness (Rms) changed from 33.8 nm for pristine NiPI to 24.6, 24.3, and 25.3 nm, respectively. Thus, coating with different TIPD concentrations did not have a significant effect on the value of the Rms. Furthermore, in the phase image of NiPI, the topographical variations of granular Ni films were expressed as a darker edge effect (Fig. 5b). After coating TIPD onto NiPI, we expected the phase changes to be more obvious at the darker edges of the granular NiPI. The previous study have been reported [17] that charge collection could be enhanced by using a thin layer of Ti/TiO_x on top of the Al electrode; in the absence of this Ti compound coating, the oxide formed on Al blocked charge transport. For our TIPD systems, even a small amount of oxygen (representing native oxides or B_2O_3) formed on the NiPI surface (Fig. 3B), we suspected that a higher concentration of the coating TIPD solution (3.75 wt%) would be more effective at enabling charge collection in the inverted cells than would a coating of 0.94 wt%. From an analysis of the PSCs' performances, we found that higher concentrations of TIPD led to improved PCE, presumably because a more uniform TIPD layer on NiPI enhanced electron transport to the anode (Fig. 5c–f). Increasing the concentration of TIPD from 3.75 to 15 wt% decreased the current density, which led to poorer performance. Based on the similar values of V_{oc} of the PT3NiPI-15, PT7NiPI-15, and PT15NiPI-15 devices (Table 3 and Fig. 6), it appears that exceeding the critical con-

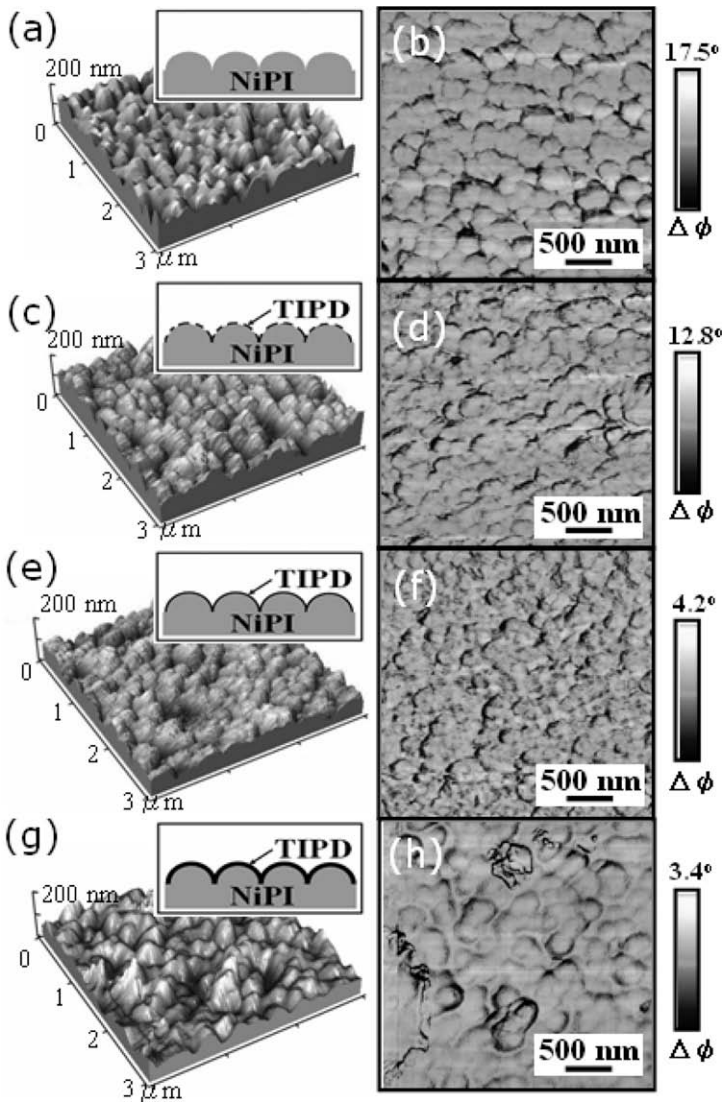

Fig. 5. (a, c, e, g) Topographies (including cartoon representations) and (b, d, f, h) phase images of NiPI and TIPD-modified NiPI films. (a, b) NiPI: pristine NiPI film; (c, d) T0NiPI: TIPD (0.94 wt%) on NiPI film; (e, f) T3NiPI: TIPD (3.75 wt%) on NiPI film; (g, h) T15NiPI: TIPD (15 wt%) on NiPI film. Scale bars, 500 nm.

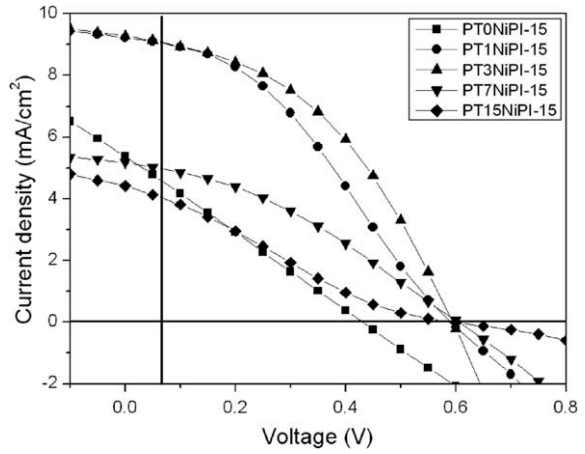

Fig. 6. *I–V* characteristics of inverted PSCs under AM 1.5 illumination (100 mW cm^{-2}).

centration of TIPD (3.75 wt%) led to a lower variation of the angles in the phase images (cf. Fig. 5g and h), which would block the degree of electron transport to NiPI and, thereby, decrease the current density.

Roman et al. [23] have reported that the light-trapping effects from active layers on the periodic Al metal nanostructures, and those structures could further enhance PSCs performance. Comparing the dimension of the granular NiPI with the Al grating structure, the NiPI films were believed to have the same effect in PSCs. To complement the observed degree of light confinement in whole devices, herein, we performed reflective UV–vis, reflection haze factor (H_R) [45] and external quantum efficiency (EQE) measurements of overall inverted PSCs process of the plane AlPI and the granular NIPI films. Fig. 7A and B showed the SEM image of planar AlPI and granular NiPI films, respectively. In the reflective UV–vis spectra of absorbance, Fig. 7C represents that the granular NiPI films were well-adapted to improve the light-trapping in 200 nm thick P3HT:PCBM cells. Based on the previous reports, [46,47] the refractive indices of PEDOT:PSS and P3HT:PCBM were 1.1–1.6 and 1.6–2.2, respectively, in the range 400–800 nm. The higher H_R was obtained from rougher NiPI structure through reflective haze factor measurements (Fig. 8A). The total internal reflection could occur where light travels from a P3HT:PCBM film with a higher refractive index to the PEDOT:PSS film with a lower refractive index. The absorption, haze factor and EQE analysis, Figs. 7C–E, C–f and 8A show that there were more light absorptions in granular NiPI of devices (PT3NiPI device) than the planar structures of electrode (PT3AlPI device) in the range of wavelengths 400–650 nm. The beam of light scattering on the granular NiPI shows better light confinements than planar AlPI of devices. Therefore, a light trapping effect were presumed by the NiPI layer in the range 400–800 nm, hence the EQE of P3HT devices show enhance-

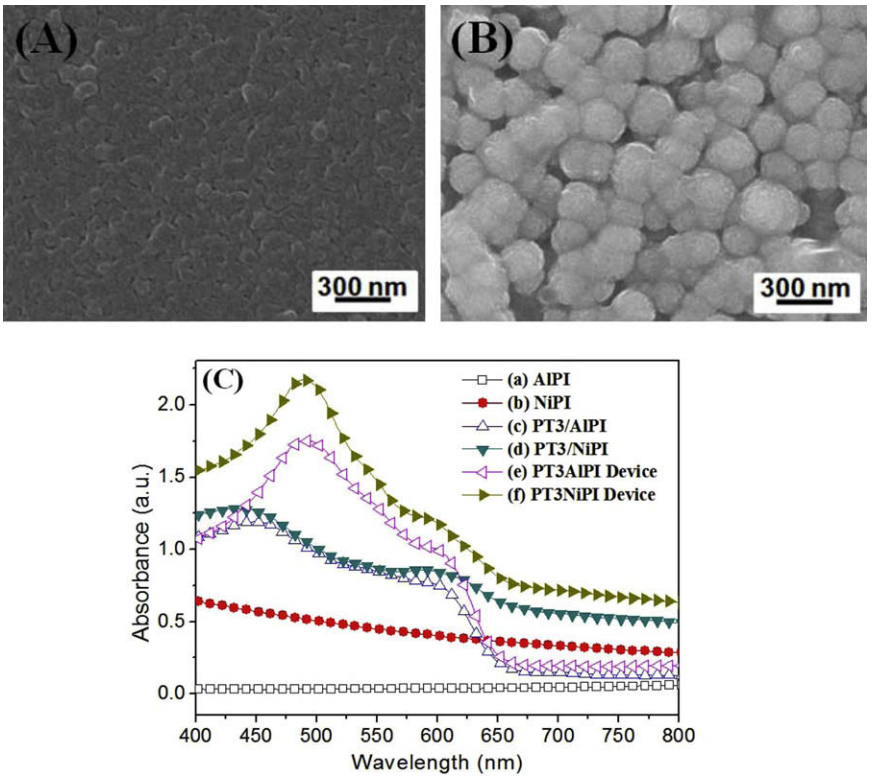

Fig. 7. SEM images (top-view) of different structure of cathodes. (A) AlPI: planar AlPI, (B) NiPI: granular NiPI. (C) Reflective UV–vis spectra of films on different structures of cathodes. (a) AlPI: planar AlPI, (b) NiPI: granular NiPI, (c) PT3/AlPI: P3HT:PCBM/TIPD(3.75 wt%)/AlPI, (d) PT3/NiPI: P3HT:PCBM/TIPD(3.75 wt%)/NiPI, (e) PT3AlPI device: PEDOT:PSS/PT3/AlPI, (f) PT3NiPI device: PEDOT:PSS/PT3/NiPI.

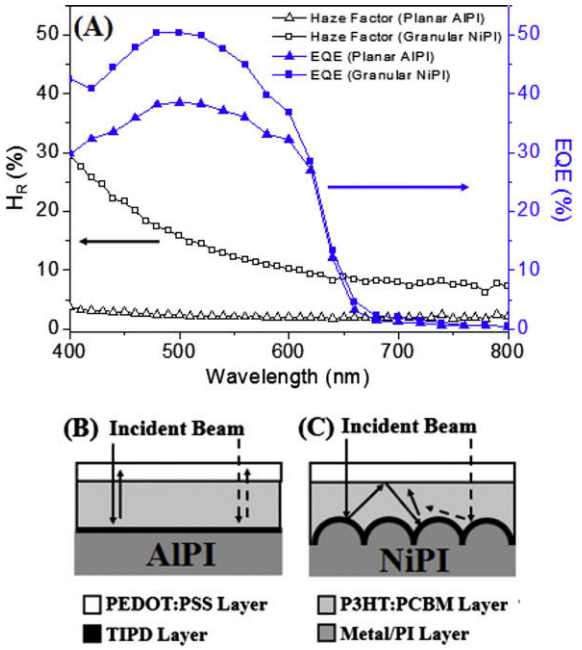

Fig. 8. (A) Reflection haze factors for different structure of cathodes and the EQE spectra of inverted PSCs on different structure of cathodes. Cartoon representations for inverted PSCs illuminated on different structure of cathodes. (B) Planar AlPI, (C) granular NiPI.

ment in the range 400–620 nm (Fig. 8A). Although different materials of cathodes may cause to the different device performance, in this study, the comparison of haze factors and EQE results, give some information of optical path length enhancement in the active layer. The Rms of coated photoactive was ca. 5.6 nm and its surface roughness was smoother than NiPI substrate (Rms ~ 33.8 nm). The cross-sectional TEM image showed the thickness of the photoactive layer was ca. 200 nm and the granular NiPI film can actually be well covered by the photoactive layer. The thin film architecture of device suggests that the variation in the film thickness would not be a problem for charge carrier extraction. As shown in Fig. 8B and C, the cartoon illustration summarized the representations of light-reflection and light-scattering properties in PSCs, and the schematic representations can be presumed that, in the active layer, rougher NiPI would induce better of light trapping than planar AlPI.

4. Conclusions

We have developed a procedure for the all-solution processing of inverted PSCs on PI substrates. In this approach, the solution processing led to the chemical formation of granular Ni thin films with high-conductivity (ca. 2777.8 S cm^{-1}) and a suitable WF for use as back contact cathodes in PSCs. We used a TIPD solution to modify the surface energy of the patterned NiPI film prior to further P3HT:PCBM coating. An analysis of the values of PCE revealed that a suitable concentration of the TIPD coating led to improved PV performance. After performing a mild oxygen plasma treatment for 5 s on the P3HT:PCBM surface, the active layer was appropriately modified for further coating with PEDOT:PSS. Moreover, we further investigated the low-temperature fabrication of high-conductivity PEDOT:PSS films by employing DMSO and ME as additives; using this approach, we obtained a high-conductivity (ca. 283.1 S cm^{-1}) HDM film after thermal treatment at just 100 °C for 5 min. The ITO-free inverted PSCs incorporating HDM films as anodes and TNiPI as the modified layer/cathodes exhibited high performance, with the PCE reaching 2.4% under AM 1.5 illumination (100 mW cm^{-2}). Although the deposition of Au grids (thickness at 100 nm) was helpful for decreasing the distance effect of PEDOT:PSS layer (hole-collection), the FF of of 0.43 is still significantly lower than the FF of 0.64 for standard devices. It was believed that higher conductivity of NiPI films and PEDOT:PSS films still need for further improving the device performance. As the results of the absorption, haze factor and EQE responses, the granular NiPI was presumed to be a better electrode/substrate through enhancing the light scattering and trapping in inverted PSCs.

Acknowledgement

We thank the National Science Council (Project NSC 97-2221-E-009-012-MY3), ROC, for financial support.

References

[1] J.Y. Kim, S.H. Kim, H.H. Lee, K. Lee, W. Ma, X. Gong, A.J. Heeger, Adv. Mater. 18 (2006) 572.
[2] S.S. Kim, S.I. Na, J. Jo, G. Tae, D.Y. Kim, Adv. Mater. 19 (2007) 4410.
[3] J.Y. Kim, K. Lee, N.E. Coates, D. Moses, T.Q. Nguyen, M. Dante, A.J. Heeger, Science 317 (2007) 222.
[4] M.D. Irwin, D.B. Buchholz, A.W. Hains, R.P.H. Chang, T.J. Marks, Proc. Natl. Acad. Sci. USA 105 (2008) 2783.
[5] C.P. Chen, S.H. Chan, T.C. Chao, C. Ting, B.T. Ko, J. Am. Chem. Soc. 130 (2008) 12828.
[6] X. Yang, J. Loos, S.C. Veenstra, W.J.H. Verhees, M.M. Wienk, J.M. Kroon, M.A.J. Michels, R.A.J. Janssen, Nano Lett. 5 (2005) 579.
[7] F.C. Krebs, K. Norrman, Prog. Photovolt: Res. Appl. 15 (2007) 697.
[8] M.S. White, D.C. Olson, S.E. Shaheen, N. Kopidakis, D.S. Ginley, Appl. Phys. Lett. 89 (2006) 143517.
[9] C. Waldauf, M. Morana, P. Denk, P. Schilinsky, K. Coakley, S.A. Choulis, C.J. Brabec, Appl. Phys. Lett. 89 (2006) 233517.
[10] G. Li, C.W. Chu, V. Shrotriya, J. Huang, Y. Yang, Appl. Phys. Lett. 88 (2006) 253503.
[11] H.H. Liao, L.M. Chen, Z. Xu, G. Li, Y. Yang, Appl. Phys. Lett. 92 (2008) 173303.
[12] R. Steim, S.A. Choulis, P. Schilinsky, C.J. Brabec, Appl. Phys. Lett. 92 (2008) 093303.
[13] T. Ameri, G. Dennler, C. Waldauf, P. Denk, K. Forberich, M.C. Scharber, C.J. Brabec, K. Hingerl, J. Appl. Phys. 103 (2008) 084506.
[14] B.Y. Yu, A. Tsai, S.P. Tsai, K.T. Wong, Y. Yang, C.W. Chu, J.J. Shyue, Nanotechnology 19 (2008) 255202.
[15] S.K. Hau, H.L. Yip, O. Acton, N.S. Baek, H. Ma, A.K.Y. Jen, J. Mater. Chem. 18 (2008) 5113.
[16] T. Nyberg, Synth. Met. 140 (2004) 281.
[17] M. Glatthaar, M. Niggemann, B. Zimmermann, P. Lewer, M. Riede, A. Hinsch, J. Luther, Thin Solid Films 491 (2005) 298.
[18] B. Zimmermann, M. Glatthaar, M. Niggemann, M.K. Riede, A. Hinsch, A. Gombert, Sol. Energy Mater. Sol. Cells 91 (2007) 374.
[19] K. Tvingstedt, O. Inganäs, Adv. Mater. 19 (2007) 2893.
[20] V. Kažukauskas, M. Pranaitis, F. Kajzar, M. Glatthaar, A. Hinsch, Mol. Cryst. Liquid Cryst. 484 (2008) 373.
[21] J. Kim, D.Y. Khang, J.H. Kim, H.H. Lee, Appl. Phys. Lett. 92 (2008) 133307.
[22] K. Tvingstedt, N.K. Persson, O. Inganäs, Appl. Phys. Lett. 91 (2007) 113514.

[23] L.S. Roman, O. Inganäs, T. Granlund, T. Nyberg, M. Svensson, M.R. Andersson, J.C. Hummelen, Adv. Mater. 12 (2000) 189.
[24] K. Akamatsu, S. Ikeda, H. Nawafune, Langmuir 19 (2003) 10366.
[25] S. Ikeda, H. Yanagimoto, K. Akamatsu, H. Nawafune, Adv. Funct. Mater. 17 (2007) 889.
[26] Y.S. Hsiao, W.T. Whang, S.C. Wu, K.R. Chuang, Thin Solid Films 516 (2008) 4258.
[27] Y. Matsumura, Y. Enomoto, M. Sugiyama, K. Akamatsu, H. Nawafune, J. Mater. Chem. 18 (2008) 5078.
[28] A. Hayakawa, O. Yoshikawa, T. Fujieda, K. Uehara, S. Yoshikawa, Appl. Phys. Lett. 90 (2007) 163517.
[29] F. Zhang, M. Ceder, O. Inganäs, Adv. Mater. 19 (2007) 1835.
[30] Z. Tan, C. Yang, E. Zhou, X. Wang, Y. Li, Appl. Phys. Lett. 91 (2007) 023509.
[31] Y.S. Hsiao, W.T. Whang, C.P. Chen, Y.C. Chen, J. Mater. Chem. 18 (2008) 5948.
[32] S.K.M. Jönsson, J. Brigerson, X. Crispin, G. Greczynski, W. Osikowicz, A.W. Denier van der Gon, W.R. Salaneck, M. Fahlman, Synth. Met. 10361 (2003) 1.
[33] B.D. Martin, N. Nikolov, S.K. Pollack, A. Saprigin, R. Shashidhar, F. Zhang, P.A. Heiney, Synth. Met. 142 (2004) 187.
[34] J. Ouyang, Q. Xu, C.W. Chu, Y. Yang, G. Li, J. Shinar, Polymer 45 (2004) 8443.
[35] J. Ouyang, C.W. Chu, F.C. Chen, Q. Xu, Y. Yang, Adv. Funct. Mater. 15 (2005) 203.
[36] J. Hung, P.F. Miller, J.S. Wilson, A.J. de Mello, J.C. de Mello, D.D.C. Bradley, Adv. Funct. Mater. 15 (2005) 290.
[37] A.M. Nardes, M. Kemerink, M.M. de Kok, E. Vinken, K. Maturova, R.A.J. Janssen, Org. Electron. 9 (2008) 727.
[38] H.L. Skriver, N.M. Rosengaard, Phys. Rev. B 46 (1992) 7157.
[39] G. Li, V. Shrotriya, Y. Yao, J. Huanga, Y. Yang, J. Mater. Chem. 17 (2007) 3126.
[40] S. Chaudhary, H. Lu, A.M. Müller, C.J. Bardeen, M. Ozkan, Nano Lett. 7 (2007) 1973.
[41] T. Aernouts, P. Vanlaeke, W. Geens, J. Poortmans, P. Heremans, S. Borghs, R. Mertens, R. Andriessen, L. Leenders, Thin Solid Films 451 (2004) 22.
[42] J.Y. Lee, S.T. Connor, Y. Cui, P. Peumans, Nano Lett. 8 (2008) 689.
[43] J. Huang, X. Wang, Y. Kim, A.J. de Mello, D.D.C. Bradley, J.C. de Mello, Phys. Chem. Chem. Phys. 8 (2006) 3904.
[44] S.I. Na, S.S. Kim, J. Jo, D.Y. Kim, Adv. Mater. 20 (2008) 1.
[45] V. Terrazzoni-Daudrix, J. Guillet, X. Niquille, A. Shah, R. Morf, A. Tishchenko, V. Brioude, O. Parriaux, D. Fischer, Mat. Res. Soc. Symp. Proc. 769 (2003) H6.14.1.
[46] F. Monestier, J.-J. Simon, P. Torchio, L. Escoubas, F. Flory, S. Bailly, R. de Bettignies, S. Guillerez, C. Defranoux, Sol. Energy Mater. Sol. Cells 91 (2007) 405.
[47] L.A.A. Pettersson, S. Ghosh, O. Inganäs, Org. Electron. 3 (2002) 143.